

# Ultrawideband Schiffman Phase Shifter Designed With Deep Neural Networks

Sensong An<sup>✉</sup>, Bowen Zheng<sup>✉</sup>, Hong Tang<sup>✉</sup>, Hang Li, Li Zhou, Yunxi Dong, Mohammad Haerinia<sup>✉</sup>, *Student Member, IEEE*, and Hualiang Zhang<sup>✉</sup>, *Senior Member, IEEE*

**Abstract**—This article presents a novel method for the forward modeling and inverse design of a class of Schiffman phase shifters using deep neural networks (DNNs). Since DNNs are capable of mapping the highly nonlinear correlations between inputs and outputs, we constructed a fully connected DNN to predict the electromagnetic (EM) responses of Schiffman phase shifters given their physical dimensions. Based on this fast and accurate modeling tool, a cascaded inverse design DNN was then built and trained to achieve instant on-demand phase shifter designs. This approach is versatile and can be easily modified to accomplish different design goals. To demonstrate its efficacy, we trained two DNNs to realize Schiffman phase shifter designs with different bandwidths (40% and 60%) and arbitrary phase shift targets (0°–180°). Simulation results and experimental verifications substantiate that their performances are comparable with the state-of-the-art designs. Moreover, we discussed the proposed methods' potential in dealing with design tasks that are nonintuitive and beyond the scope of the existing approaches. We envision that this DNN approach can be extended to the design of various EM components including but not limited to antennas, filters, power dividers, and frequency selective surfaces (FSS).

**Index Terms**—Deep learning, deep neural networks (DNNs), inverse design, Schiffman, wideband phase shifter.

## I. INTRODUCTION

PHASE shifters play an important role in beam scanning phased arrays, modulators, and wireless communication systems. Ideal phase shifters should provide flat phase shift over wide operating frequency band with low loss. Among various types of differential phase shifters, those realized in planar technology, either stripline [1], microstrip line [2], or substrate integrated waveguide (SIW) [3] are widely adopted due to their low cost, small amplitude imbalance, and wide-bandwidth characteristics. In general, wideband planar phase shifters can be characterized into several categories: Schiffman phase shifters [1], [2], [4]–[12], loaded-line phase

Manuscript received 28 December 2021; revised 11 March 2022, 2 May 2022, and 8 June 2022; accepted 3 July 2022. Date of publication 22 July 2022; date of current version 4 November 2022. This work was supported in part by the Office of Naval Research (ONR). (Corresponding author: Hualiang Zhang.)

Sensong An was with the Department of Electrical and Computer Engineering, University of Massachusetts at Lowell, Lowell, MA 01854 USA. He is now with the Department of Material Science and Engineering, Massachusetts Institute of Technology, Cambridge, MA 02142 USA (e-mail: ssan@mit.edu).

Bowen Zheng, Hong Tang, Hang Li, Li Zhou, Yunxi Dong, Mohammad Haerinia, and Hualiang Zhang are with the Department of Electrical and Computer Engineering, University of Massachusetts at Lowell, Lowell, MA 01854 USA (e-mail: hualiang\_zhang@uml.edu).

This article has supplementary material provided by the authors and color versions of one or more figures available at <https://doi.org/10.1109/TMTT.2022.3189655>.

Digital Object Identifier 10.1109/TMTT.2022.3189655

shifters [13]–[18], broadside coupling phase shifters [19]–[21], and others [22]–[24]. Compared with their counterparts, the Schiffman phase shifters are compact in size and easy to fabricate using print circuit board (PCB) technology, while still provide accurate phase shift in relatively wide bandwidth (usually >50%), making them stand out from various wideband phase shifter designs.

The original Schiffman phase shifters are based on stripline structures [1]. When applying the design approach to the microstrip circuits, the uneven phase velocity of odd and even modes of the coupling region led to impedance mismatch and hence large insertion loss. Different approaches were discussed to solve this problem, including introducing the multisection coupled lines [4], adopting advanced analysis method which calculates the actual phase velocities [6], and removing part of the ground to reduce the even mode phase velocity [7]. Analytical equations for approximate calculations were presented in these works, which can be used to guide the design. However, due to the approximations being used and the unquantifiable influence of different structures (e.g., chamfered entries, fringing effects, and parasite inductances of the narrow links between coupled lines), it is hard to analytically calculate the electromagnetic (EM) response of a Schiffman phase shifter given its dimensions. As a result, time-consuming fine-tuning is always required in the design process.

Machine learning (ML) techniques, especially the artificial neural networks (ANNs) have been recognized as an powerful tool to address this issue, and were widely adopted for the modeling, optimization, and/or inverse design of microwave components and circuits such as transitions [25], ground via [26], amplifiers [27], transmission line [28], and filters [29]–[35]. Among these works, Watson *et al.* presented a knowledge-based ANN approach for the modeling of microstrip grounding via coplanar waveguide (CPW) structures and stripline-to-stripline transitions [25], [26]. Zhang *et al.* proposed an ANN-based CAD (computer-aided design) approach for the modeling and optimizations of FET, CPW filters, and patch antennas [27], [30], [31]. Delgado *et al.* presented a SYNTHESIS-ANN for the modeling of structures including microstrip line and printed antennas with balun [28]. In [29], Zhang *et al.* proposed an ANN approach for the optimization of a bandstop microstrip filter. Na *et al.* introduced ANNs for the parameter extraction and modeling of various types of filters [32]–[35]. With the ANNs adopted in these works, conventional time-consuming full-wave simulation and

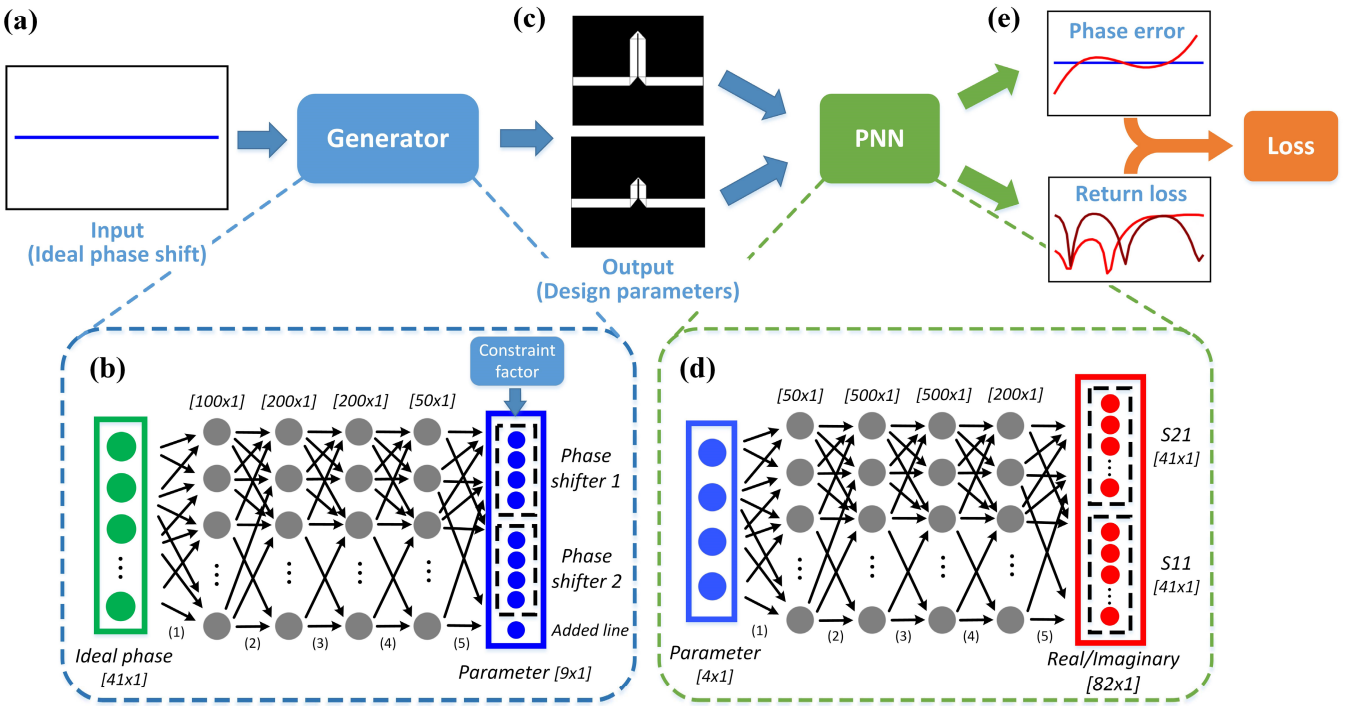


Fig. 1. Architecture of the wideband phase shifter design network. (a) Ideal spectral phase shift responses designated as input of the tandem network. (b) The phase shifter model generator (the “generator”) that constructed with four hidden layers. (c) Output of the generator, composed of the design parameters of two phase shifters and the length of added transmission line. (d) The pretrained PNN calculates the accurate transmission and reflection coefficients with given design parameters of the phase shifter. (e) Phase error and return loss are calculated and minimized during the training of the tandem network.

parametric modeling process can be substituted (and carried out) with a fully trained network on a one-time calculation basis, and thus greatly reducing the overall modeling and design time.

In recent years, deep neural networks (DNNs) have been widely adopted in various fields such as computer vision (CV), natural language processing (NLP), and computational learning. They have surpassed human performance in terms of both accuracy and efficiency in different tasks, including self-driving systems, efficient web search, and optical character recognition. Moreover, the DNNs are usually composed of more hidden layers compared with the ANNs, which makes them well suited to solve the EM forward modeling and inverse design problems, due to their ability to map the highly nonlinear relationships between the inputs (physical quantities) and outputs (EM fields or responses). The existing works have successfully demonstrated the feasibility to employing different DNNs to address the forward characterization and inverse design of metamaterials [36], [37], metasurfaces [38]–[40], microwave antennas [41], [42], and filters [43], [44]. The DNNs constructed in these works successfully unveiled the hidden relationship between inputs and outputs, meanwhile addressed the high-dimensional inputs challenge that cannot be easily tackled with a shallow ANN [43], [44].

In this article, we show how a DNN based on concise fully connected architecture can be utilized for the fast forward modeling and inverse design of microwave components. Due to the capability of mapping the highly nonlinear relationships between inputs and outputs, the DNNs are capable of

predicting accurate phase and amplitude responses of an EM component given its design parameters. Once fully trained, the DNNs can generate the prediction results in milliseconds, and thus enabling fast on-demand designs. Without loss of generality, a class of microstrip Schiffman phase shifters are explored for the purpose of demonstration. For the first time, a predicting neural network that is capable of simultaneously modeling the phase shift, insertion loss, and return loss of Schiffman phase shifters over a relatively wide spectrum (133%) has been demonstrated. Based on the highly accurate forward predicting network, a tandem inverse design network was constructed for the fast on-demand designs of Schiffman phase shifter with arbitrary phase shift and bandwidth targets. To verify the efficacy of the proposed approach, two groups of phase shifter designs, with 60% and 40% bandwidth, respectively, were designed, fabricated, and measured. The good agreement between design targets and measurement results substantiate that the proposed approach accomplished two important goals in the field of EM component design: 1) building a fast and accurate simulation tool to validate the performance of EM components and 2) generating the layout of on-demand designs instantly, with no further optimization and fine-tuning needed. It is expected that the proposed approach can be easily generalized to other EM problems, including but not limited to antenna design, microwave circuit design, and EM compatibility problems.

## II. NETWORK STRUCTURE

The proposed wideband phase shifter design network is illustrated in Fig. 1. The design goal is to generate differential

phase shifters with user-defined phase profile while maintaining low return loss and insertion loss. Since it is possible to have multiple different devices with similar EM responses, constructing a simple inverse design network with target responses assigned as input and design parameters as output will cause the network unable to converge [33], [38], due to the conflicting input–output data pairs in the design pool. To address this problem, a “tandem” network architecture [37], [38] is adopted, which consists of an inverse design model generator (hereinafter called the “generator”) and a predicting neural network (hereinafter called the “PNN”) to form a cascaded architecture. The input and output for a “tandem” network are both EM responses, which eliminates the possibilities of nonunique solutions and thus stabilizes the training process. As shown in Fig. 1(a), the ideal spectral phase response is discretized into a 1-D vector, with all data points evenly distributed in the spectrum of interest. The generator in Fig. 1(b) consists of four consecutive fully connected hidden layers each containing 100, 200, 200, and 50 hidden neurons, respectively. The generator takes the ideal phase shift as input and generates the design parameters of two phase shifters [see Fig. 1(c)], which produce the on-demand differential phase shift. The design parameters are then designated as input for a fully trained PNN [see Fig. 1(d)], where the two phase shifters’ transmission and reflection coefficients are evaluated when passed through four full-connected hidden layers consisting of 50, 500, 500, and 200 hidden neurons, respectively. Finally, the network calculates a combined loss function [see Fig. 1(e)], which is a weighted sum of the phase error and the return loss. During the training, the weights and biases in the hidden layers of the generator are optimized to minimize this loss, while the parameters in the previously trained PNN (including weight and bias) remain unchanged. As a result, the generator becomes “smarter” as training proceeds, eventually able to generate on-demand Schiffman phase shifter designs on a one-time calculation basis.

#### A. Forward Prediction

In order to enable the inverse design, a PNN [as shown in Fig. 1(d)] is trained first to realize the fast and accurate evaluation of Schiffman phase shifters. The PNN functions as a powerful alternative to the full-wave simulation tool. It is considered as the key building block in the tandem network structure for two reasons.

1) The generator relies on the PNN to distinguish the bad designs from the good ones and thus help the generator choose the right gradient descend direction and become “smarter” in design during the training. An inaccurate PNN will eventually lead to a defective generator even after fully trained.

2) During the training of the generator, each generated phase shifter design needs to be quickly evaluated to derive the training loss. Thousands of designs are generated and evaluated during one training iteration, which is normally done in seconds. This time efficiency is only possible with a fully trained PNN.

As shown in Fig. 2(a), four design parameters including the length and width of the coupled microstrip lines and the

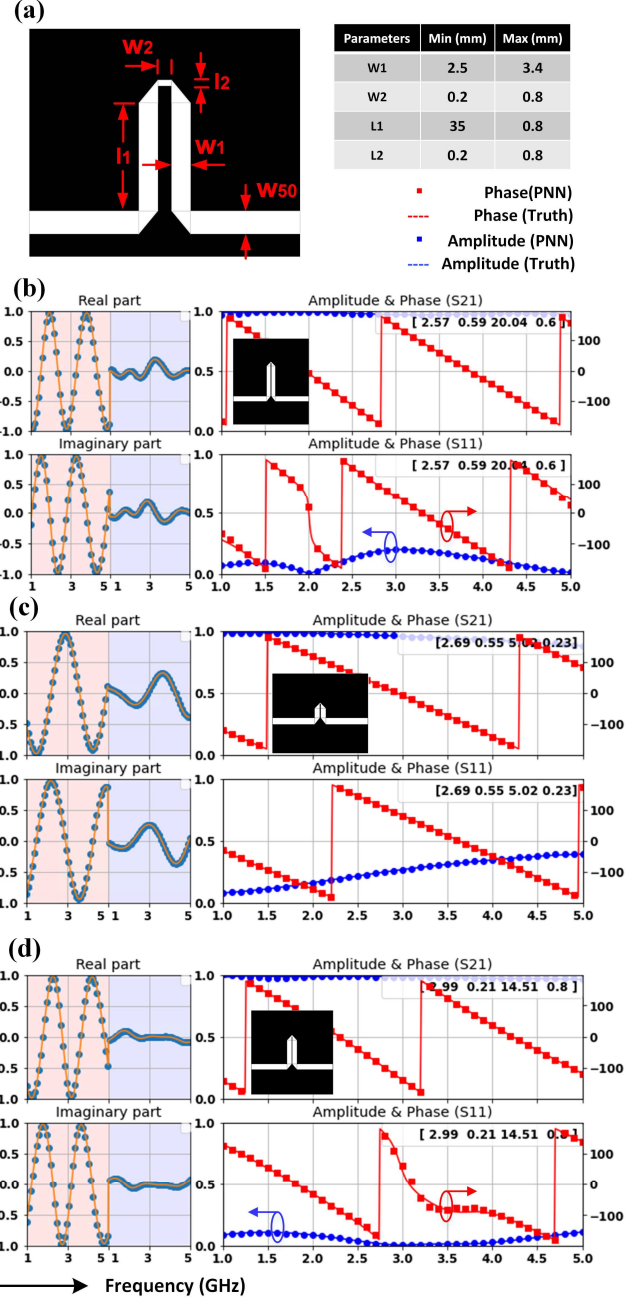


Fig. 2. PNN for Schiffman phase shifters. (a) Top-view figure showing the dimensions that parameterize the Schiffman phase shifter structure. (b)–(d) Examples of EM responses of Schiffman phase shifters predicted by the PNN (dots) and full-wave numerical simulations (lines). The real and imaginary parts of the predicted complex transmission coefficients are shown on the left in each subplot, including the reflection coefficients and transmission coefficients. Design parameters are given as insets in the following order:  $W_1$ ,  $W_2$ ,  $L_1$ , and  $L_2$  (in mm).  $W_{50}$  denotes the width of the 50- $\Omega$  transmission line.

connection section were used to parameterize the Schiffman phase shifter structures. Without loss of generality, we chose Rogers R4003C ( $\epsilon_r = 3.55$ ,  $\tan\delta = 0.0027$ ) with the thickness of 1.524 mm as the substrate. The spectra of interest are set to be from 1 to 5 GHz with center frequency at 3 GHz. To train the PNN, a dataset containing over 53 000 random Schiffman phase shifters, along with their transmission and reflection coefficients, was created using commercial software package

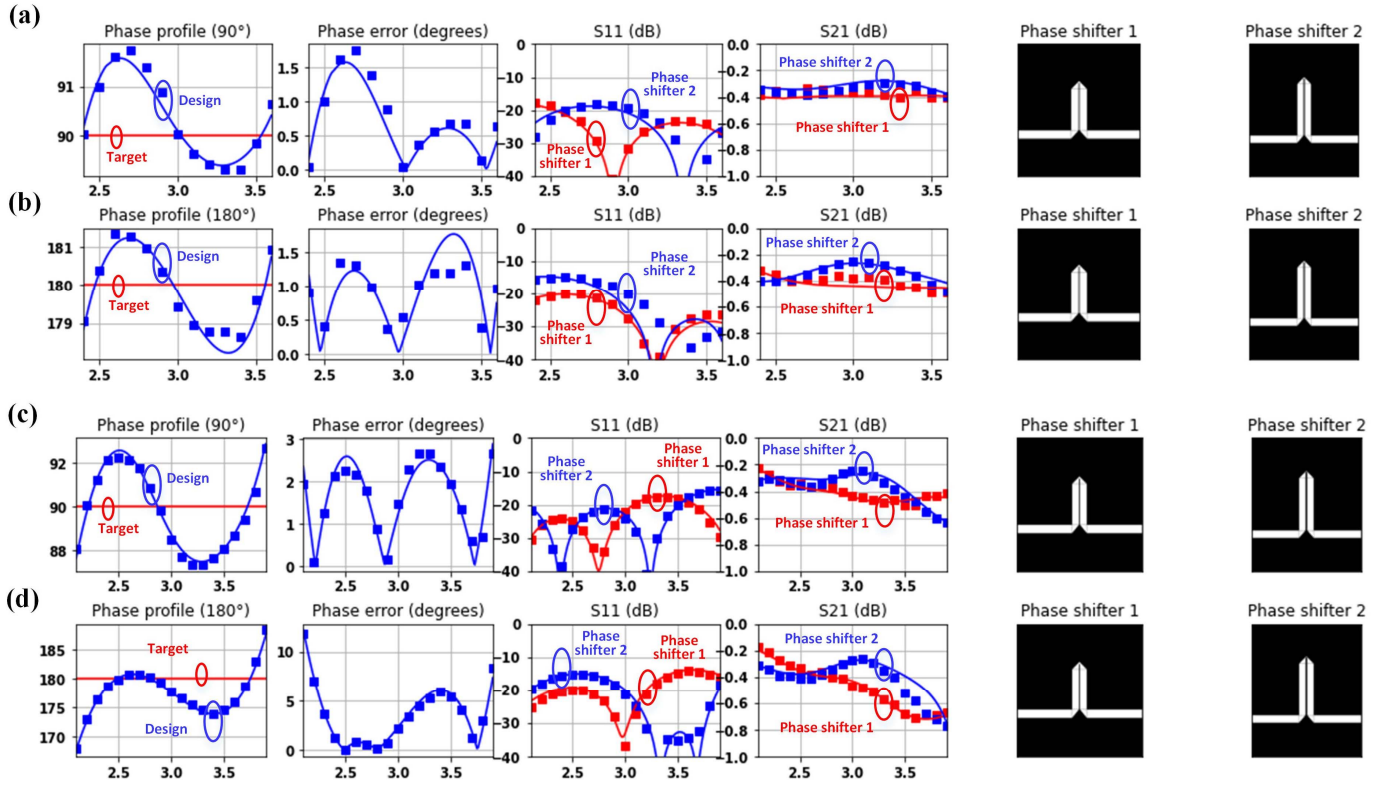


Fig. 3. Phase-shifter examples designed by the fully trained generators. (a) 90°, 40% bandwidth. (b) 180°, 40% bandwidth. (c) 90°, 60% bandwidth. (d) 180°, 60% bandwidth. Dotted lines are the PNN-predicted responses based on the designs given by the generator, and solid lines are the numerically simulated responses.

CST Microwave Studio. Among them, 70% were assigned to be the training set, while the remaining 30% were used as the test set. The whole spectrum is down-sampled into 41 frequency points (between 1 and 5 GHz) with a frequency step of 0.1 GHz, corresponding to 41 coefficients which are specified as the network output. To reduce the training complexity, the transmission and reflection coefficients are combined into the output of the PNN, which were predicted at the same time. Two independent neural networks were constructed to predict the real and imaginary parts of the coefficients, respectively. The loss functions we used for PNNs are

$$L_{\text{PNN}} = \frac{1}{N} \sum_{i=1,2,\dots,N} (S_{\text{PNN}} - S_{\text{truth}})^2 \quad (1)$$

where  $S$  is the spectral responses. After fully trained, the test set error of the real and imaginary PNNs is  $1.6 \times 10^{-5}$  and  $1.3 \times 10^{-5}$ , equivalent to a phase error of 0.1° and amplitude error of 0.005 at a single frequency point. Several prediction samples were randomly selected from the test dataset and showcased in Fig. 2, while more prediction samples are presented in Appendix Fig. 9. These examples show excellent consistency between numerical simulations and PNN predicted results across the full spectrum. Due to its one-time calculation nature, the fully trained PNNs are capable of modeling the performances of different Schiffman phase shifters with almost no time cost (e.g., in milliseconds), which enables the fast inverse design when cascaded with optimization algorithms or DNNs (as will be discussed in the next section).

### B. Inverse Design

To demonstrate the versatility of the proposed approach, two generators that are capable of designing Schiffman phase shifters with two different preassigned fractional bandwidths (40% and 60%) were trained. The same dataset was used during these two training processes, which contains randomly generated ideal flat phase shift targets ranging from 0° to 180°. Since the inputs are not labeled with corresponding design parameters, the training was executed in an unsupervised way. The output layer contains nine values, including the design parameters of two differential phase shifters ( $W_1$ ,  $W_2$ ,  $L_1$ , and  $L_2$  for each phase shifter) and the length of an extra 50-Ω transmission line cascaded to the first phase shifter which is used to adjust the phase shift value. With the help of the fully trained PNN, the insertion loss, phase, and return loss of both phase shifters, along with the differential phase shift between them can be instantly calculated. The loss functions of the cascaded network can be expressed as the weighted sum of three least square errors, including a phase error term, a constraint factor term, and a return loss term

$$L_{\text{Generator}} = \sum A \cdot (S_{\text{PNN}} - S_{\text{target}})^2 + B \cdot (P - P_{\text{clipped}}(\max, \min))^2 + C \cdot (\text{ReLU}(S_{11} - \text{threshold}))^2 \quad (2)$$

where  $A$ ,  $B$ , and  $C$  are the weight coefficients;  $S_{\text{PNN}}$  and  $S_{\text{target}}$  are the actual phase shift of current design and the target phase shift, respectively.  $P$  is the output vector [see Fig. 1(c)] containing design parameters and  $P_{\text{clipped}}$  is a

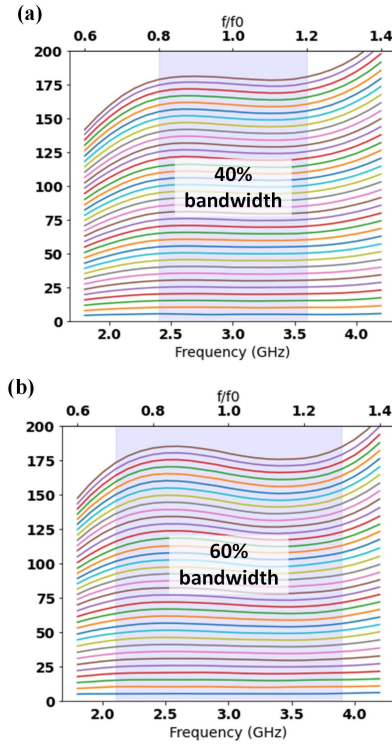


Fig. 4. More phase shifter designs by the fully trained generators. Performance of 36 Schiffman phase shifters with design targets ranging from  $5^\circ$  to  $180^\circ$  ( $5^\circ$  interval). (a) Designs by the 40% bandwidth generator. (b) Designs by the 60% bandwidth generator.

vector with all values in  $P$  clipped to a preset maximum and minimum value [see Fig. 2(a)]. Since the accuracy of the PNNs is only guaranteed within the preset data range, a constraint factor [second term in (2)] was added to the loss function, which measures the distance from output to the desired parameter value range. When the vector  $P$  falls out of the preset value range, the increasing loss function value will force the optimizer to regress to generate a  $P$  value within the desired range (max, min). When the return loss of the generated design is higher than the preset threshold (set to be  $-14$  dB during training), the third term in (2) will generate an error larger than zero and force the optimizer to generate a different design with lower return loss. Since the second and third terms in (2) should be equal to zero with an ideal phase shifter design, their corresponding weight coefficient is set to be a much larger value ( $A = 1$ ,  $B = C = 500$ ). After 20000 iterations of training for each group of data, the combined error eventually stabilized at 0.84 and 7.85 for 40% bandwidth targets and 60% bandwidth targets, respectively (details can be found in the Appendix Fig. 8 and Table I). The larger error for 60% bandwidth targets manifests the increasingly design difficulty of Schiffman phase shifters with a larger bandwidth. Fig. 3 shows four representative design examples, including two  $90^\circ$  and two  $180^\circ$  phase shifters designed by both generators. The relatively low phase error ( $90^\circ \pm 1.6^\circ$ ,  $180^\circ \pm 2^\circ$  designed by the 40% bandwidth generator;  $90^\circ \pm 3^\circ$ ,  $180^\circ \pm 12^\circ$  designed by the 60% bandwidth generator) indicates the good efficacy of the proposed deep learning approach.

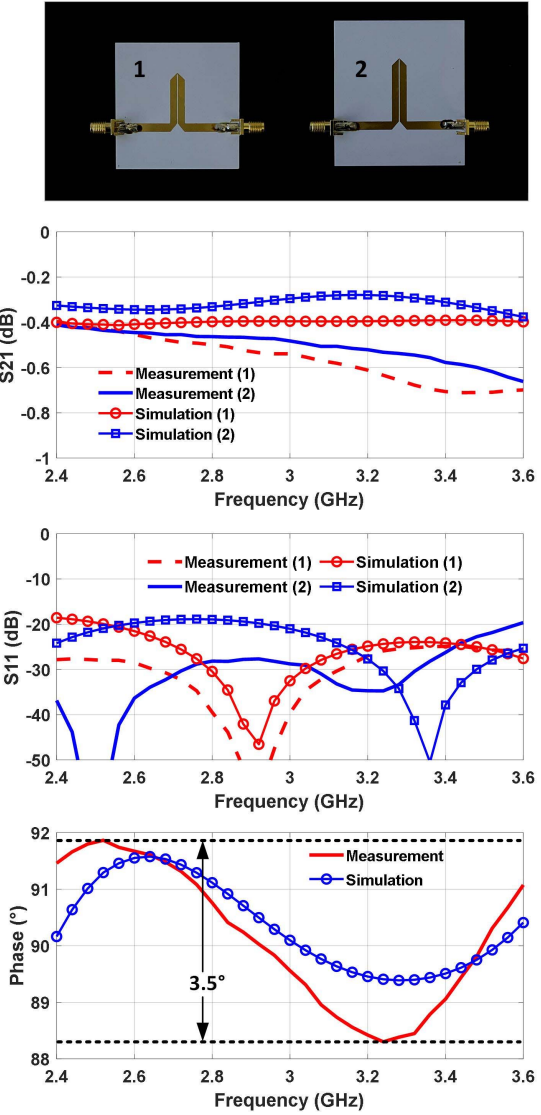


Fig. 5. Measurement results of the  $90^\circ$  Schiffman phase shifters with 40% fractional bandwidth.

As mentioned earlier, the highly efficient nature of this DNN approach allows us to generate high-performance phase-shifter designs with almost no time cost. To demonstrate this unique feature, as showcased in Fig. 4, 36 phase-shifter designs with phase shift targets ranging from  $5^\circ$  to  $180^\circ$  (with  $5^\circ$  interval) were designed using the 40% bandwidth and 60% bandwidth generators, respectively. The corresponding differential phase shifts were evaluated with the PNNs. It is worth to mention that all designs in Fig. 4(a) and 4(b) were generated and characterized within milliseconds.

### III. EXPERIMENTAL VERIFICATION

In order to verify the proposed method, two  $90^\circ$  differential phase shifters presented in Fig. 3(a) and 3(c) were fabricated and measured. Detailed parameters of these two designs are given in Appendix Table II. The substrate for the microstrip line is Rogers RO4003C with the dielectric constant of 3.55, to keep consistency with the setups used during the data collection process. The measured return loss, insertion loss, and

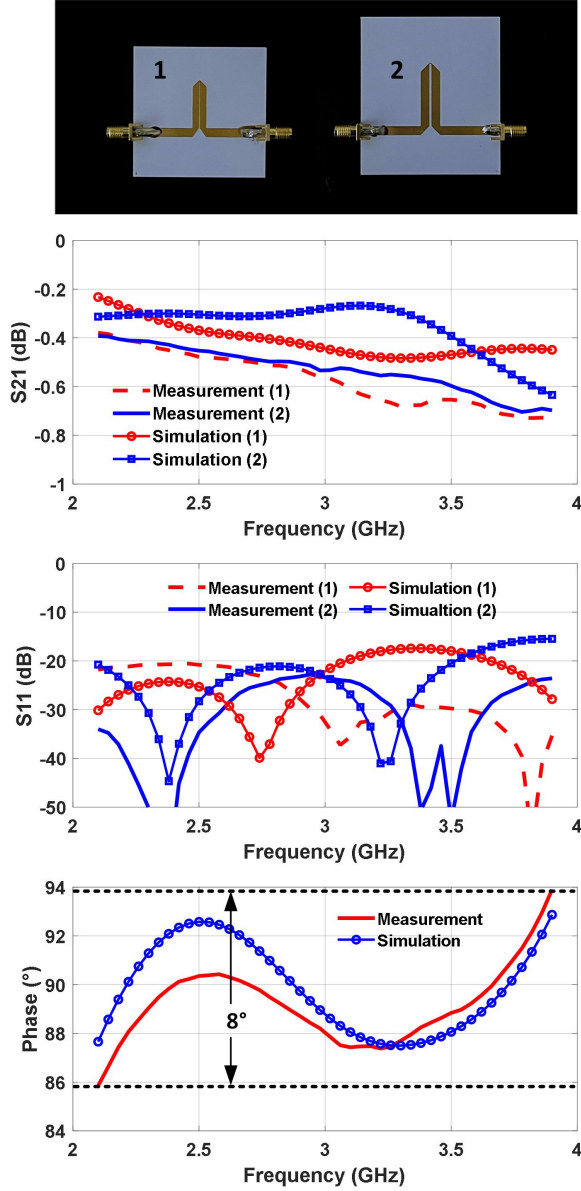


Fig. 6. Measurement results of the 90° Schiffman phase shifters with 60% fractional bandwidth.

differential phase shift of the two phase shifters are presented in the subplots of Figs. 5 and 6. The recorded minimum return loss, maximum insertion loss, and maximum phase error are 19.64 dB, 0.71 dB, and  $\pm 1.86^\circ$  for the 40% bandwidth (2.4–3.6 GHz) phase shifter and 20.68 dB, 0.73 dB, and  $\pm 4.1^\circ$  for the 60% bandwidth (2.1–3.9 GHz) phase shifter. As shown in Figs. 5 and 6, the full-wave simulation results are also included as reference. The measured results are in reasonably good agreement with the simulation results, which validates both the accuracy of the pretrained PNN and the efficacy of this inverse design approach.

#### IV. FURTHER DISCUSSION

This deep learning approach shows its unique advantages over conventional methods when dealing with designs with more degrees of freedom. As discussed in the literature, the phase errors in microstrip Schiffman phase shifters caused by

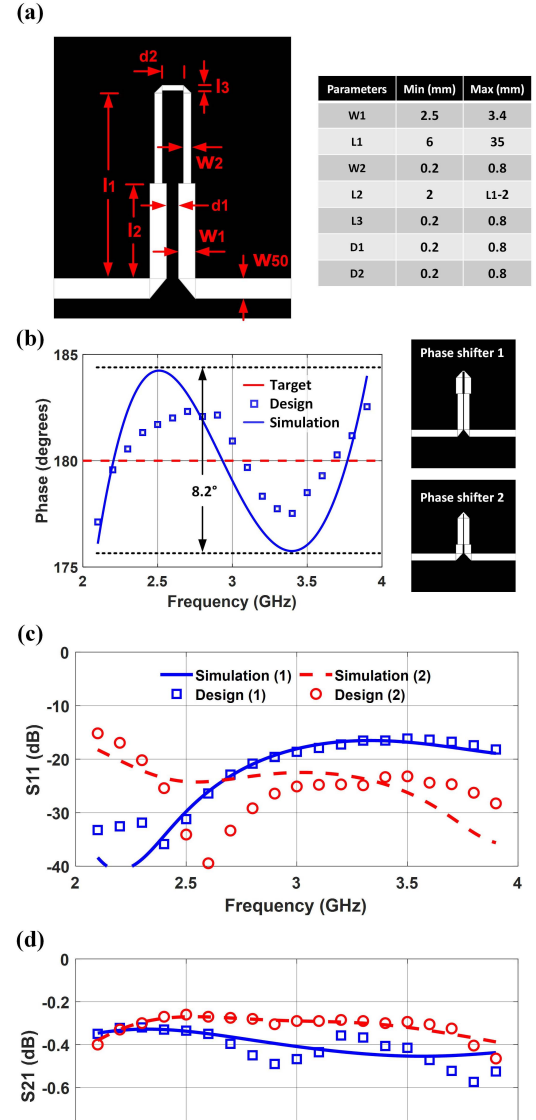


Fig. 7. 180° dual-section Schiffman phase shifter design with 60% fractional bandwidth. (a) Top-view figure showing the dimensions that parameterize the dual-section Schiffman phase shifter structure. (b) Diagram of the designs and corresponding phase shift. (c) Return loss. (d) Insertion loss. Dotted lines are the PNN-predicted responses based on the designs given by the generator, and solid lines are the numerically simulated responses.

the uneven phase velocity of odd and even modes can be moderated by applying measures such as introducing multisection coupled lines [4], adopting advanced analysis method [6], and modifying the ground plane [7], which all resulted in complex architectures that are extremely hard (if not impossible) to model with traditional field and circuit analytical solutions. Therefore, these improved designs are derived with either particular solution based on presumptions that limited the design degrees of freedom [4], or trial-and-error method which requires time-consuming fine-tuning process [7]. In contrast, the proposed prediction and inverse design process with DNNs are data-driven. With hidden layers that provide sufficient hidden units, the presented DNNs are able to uncover the highly nonlinear hidden relations between inputs and outputs, even the complicated ones that are unable to be modeled with analytical equations, according to the universal approximation

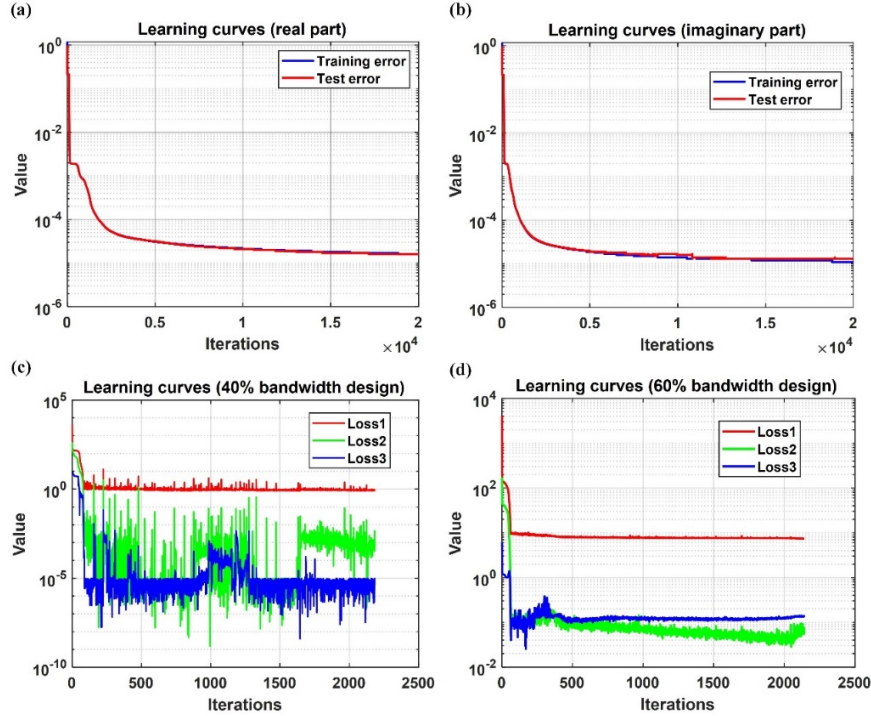


Fig. 8. Learning curves of the PNNs and model generators. Shown in the figures are the learning curves of (a) real part PNN, (b) imaginary part PNN, (c) phase shifter generator with 50% fractional bandwidth, and (d) phase shifter generator with 60% fractional bandwidth. Loss 1, 2, and 3 correspond to the first, second, and third terms in (2), respectively.

theorem [45], [46]. As a result, given sufficient amount of training data, PNNs with similar network structures can be used to model different types of structures, regardless of their complexities. To explore the proposed approach's potential in dealing with more complicated geometries, we trained another PNN and generator for the forward modeling and inverse design of a dual-section Schiffman phase shifter. As shown in Fig. 7(a), the phase shifter with dual-section coupled line structure can be parameterized into seven parameters, including the length, width of the coupled lines, and the gap between them. The network architecture in Fig. 1 was slightly modified for the training of the PNN and the model generator for dual-section Schiffman phase shifters. Specifically, we change the output size of the generator to 15 by 1 and the input size of the PNNs to 7 by 1. Over 60 000 groups of training data were then collected with the parameters randomly generated within the preset value range in Fig. 7(a). After fully trained, the combined error finally stabilized at the value of 1.98 with the same loss function in (2). Compared with the single-section generator with the final error of 7.85, this significantly lower error value clearly indicates that Schiffman phase shifters with better performance can be achieved with this dual-section structure. We then used the fully trained dual-section generator to design a 180° phase shifter with 60% fractional bandwidth (design details are included in Appendix Table III). The design diagram, phase, return loss, and insertion loss of the proposed design are shown in Fig. 7(b)–(d), respectively. Compared with the 180° phase-shifter design in Fig. 3(d), this dual-section design was able to reduce the phase error by 60% while maintaining similar level of return loss and insertion

loss, which clearly indicates the advantage of introducing more design degrees of freedom.

A major concern for this data-driven design approach is the time-consuming data collection process. We want to point out that the capability of the inverse design network actually depends on the forward prediction network (PNN). As for the design examples included in this article, since operation frequency of the PNN is from 1 to 5 GHz, the generator can be trained to generate inverse designs with different center frequencies, as long as the operating frequency band falls within the 1–5 GHz range. For example, we have also trained a generator for the design of phase shifters with center frequency equals to 4 GHz (supporting information Section I). To deal with designs that work at different frequency bands, new datasets need to be collected to train the PNNs. Fortunately, unlike other regression or classification problems in the deep learning field, the data in EM design problems are cheap and easily accessible, with the majority of the cost coming from the electricity consumption and the time cost while conducting numerical simulations. It is also worth noting that the data collections in this article are done in an unsupervised way, and this process can be easily accelerated by running the simulations in parallel. For example, it took 3 and 4 days to collect enough amount of training data for the PNNs in Figs. 2 and 7 with an 8-node cluster, respectively.

## V. CONCLUSION

To conclude, we have proposed a novel DNN-based approach for the inverse design of high-performance Schiffman phase shifters. Based on the tandem architecture, we have

TABLE I  
HYPERPARAMETERS USED DURING THE TRAINING OF PNN AND PHASE-SHIFTER GENERATOR

Hyper-parameters	PNN		Phase shifter Generator		
	Single section	Dual section	40% Bandwidth, Single section	60% Bandwidth, Single section	60% Bandwidth, Dual section
<b>Training set size</b>	37,100	42,000	50,000	50,000	50,000
<b>Test set size</b>	15,900	18,000	/	/	/
<b>Optimizer</b>	Adam	Adam		Adam	
<b>Learning rate</b>	10-5	10-5		10-4	
<b>Batch size</b>	200	200		200	
<b>Batch Norm.</b>	No	No		No	
<b>Nonlinear activations</b>	ReLU	ReLU		ReLU	
<b>Iterations</b>	20,000	20,000	2,200	2,200	3,000
<b>Time taken</b>	2 h	2 h	15 min	15 min	17 min
<b>Error (train)</b>	1.6E-5(real) 1.1E-5(imag)	4.3E-5(real) 3.2E-5(imag)	0.84	7.85	1.98
<b>Error (test)</b>	1.6E-5(real) 1.3E-5(imag)	9.8E-5(real) 1.2E-4(imag)	/	/	/

demonstrated the fast and accurate forward characterization and inverse design of a class of Schiffman phase shifters. Several design examples, including two 90° phase shifters and two 180° phase shifter with 40% and 60% fractional bandwidth, were designed and numerically verified. Performances of the DNN-generated designs are comparable with the state-of-the-art [7], [15], [47], [48]. A detailed performance comparison with several reported wideband phase shifters is included in supporting information Section III.

This deep learning approach not only quickly explores the locally optimal designs for given structures but also eliminates the fine-tuning process that was increasingly time-consuming in structures with complicated shapes. Different from traditional design approaches or local optimization algorithms, the presented DNNs process the input data in parallel, thus the training and design time of the PNNs and generators are not affected by the number of parameters, making them suitable for the inverse design of multiparameter problems. We believe that the proposed method is unique and stands out from the previous DNN approaches because 1) the formulation of DNN-based phase-shifter forward modeling is capable of predicting not only the spectral transmittance and reflectance but also the accurate phase responses, which enables the inverse design of devices with phase profile-related targets including microwave circuits, phase shifters, and feeding networks; and 2) we have carefully engineered the loss function of the inverse design network and proposed a novel way to apply multiple restrictions simultaneously: within the target frequency band, the phase error is minimized; the reflection is controlled below a certain threshold ( $-14$  dB in the examples), and all dimensions are generated within the preset ranges (to ensure the prediction accuracy). Considering that the design targets of modern EM devices are usually complicated and combinations of multiple requirements, the ability to reconcile multiple design targets helps to pave the way for extending this approach to the design of other EM devices.

Although this article mainly discusses the forward modeling and inverse design of Schiffman phase shifters, the deep learning approach for objective-driven design developed herein is not limited to specific phase shifter or device categories. With customized loss functions and training datasets, the proposed framework can be adapted to the design of various EM components that can be defined with several design parameters, including but not limited to antennas, filters, power dividers, and frequency selective surfaces (FSS). As a quick demonstration, an inverse design DNN example that is able to generate designs based on target reflectance is included in the Supporting Information Section II. Moreover, by adopting the convolutional neural network (CNN) layers, the PNN can deal with image input [39], which further increases its adaptability.

## APPENDIX

In the Appendix, we provide further details on network modeling, network training, and additional examples showcasing the performances of different networks. This Appendix comprises the following sections.

### A. Hyperparameters Used During DNN Training Process

Hyperparameters used in the training for both PNNs and all three generators are shown in Table I. The hardware consists of a quad-core CPU with 3.5-GHz clock speed, 64 GB of RAM, and two Nvidia 1080Ti GPUs. As shown in the table, after 20 000 iterations, the average test set error for single section PNNs stabilized at 0.000016 and 0.000013 for the real and imaginary parts, respectively. The final test error for dual-section PNNs is 0.000098 for the real parts and 0.00012 for the imaginary parts, respectively. With the current hardware setup, the training takes 4 h for all four PNNs before their error rates stabilize (Fig. 8). The model generator networks, on the other hand, takes less training

TABLE II  
DETAILED DIMENSIONS OF THE PHASE-SHIFTER DESIGNS IN FIG. 3

Unit: mm	Phase shifter #1				Phase shifter #2				Additional 50Ω line
	W1	W2	L1	L2	W1	W2	L1	L2	
90° (40% BW)	3.03	0.38	16.78	0.56	2.91	0.45	23.51	0.34	2.12
180° (40% BW)	3.07	0.2	14.24	0.7	2.5	0.2	27.59	0.2	4.6
90° (60% BW)	2.87	0.23	16.2	0.73	2.94	0.78	23.68	0.21	-0.37
180° (60% BW)	2.5	0.2	13.26	0.55	2.51	0.2	28.45	0.21	-0.43

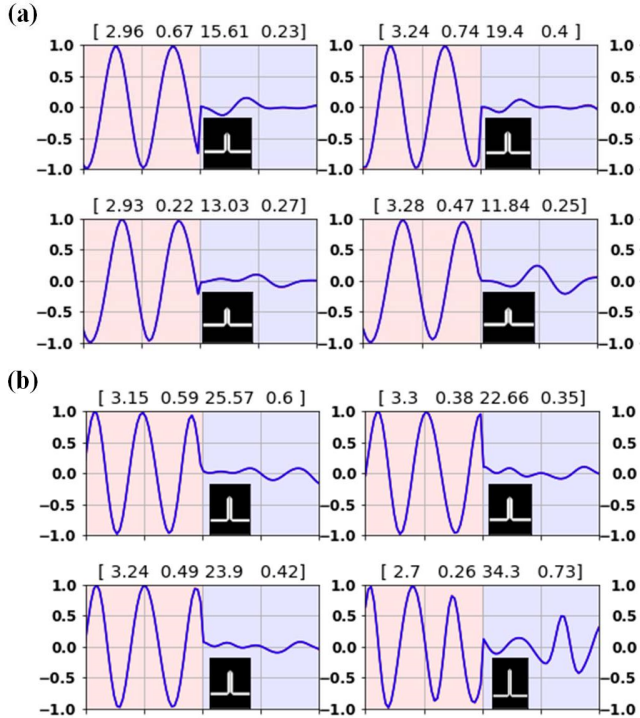


Fig. 9. Additional prediction examples generated with the single-section PNNs. (a) Real part prediction examples. (b) Imaginary part prediction examples.

time due to the smaller network dimensions and less non-intuitive inverse design rules. All three generators are fully trained after less than 3000 iterations, each requiring less than 20 min.

#### B. Additional Samples of the PNN for Single-Section Schiffman Phase Shifters

In As shown in Fig. 9, in each panel, the red curve represents the PNN predicted values. The blue curves depict numerically simulated values obtained with the commercial frequency domain solver (CST Microwave Studio). Reflection coefficients are highlighted in orange and transmission coefficients are highlighted in cyan. Randomly generated design parameters, including  $W_1$ ,  $W_2$ ,  $L_1$ , and  $L_2$  (in mm), are shown at the top of each panel (in the above order). Please note that the predicted values are barely seen in the plots since they are mostly overlapped with the ground truth due to the high accuracy.

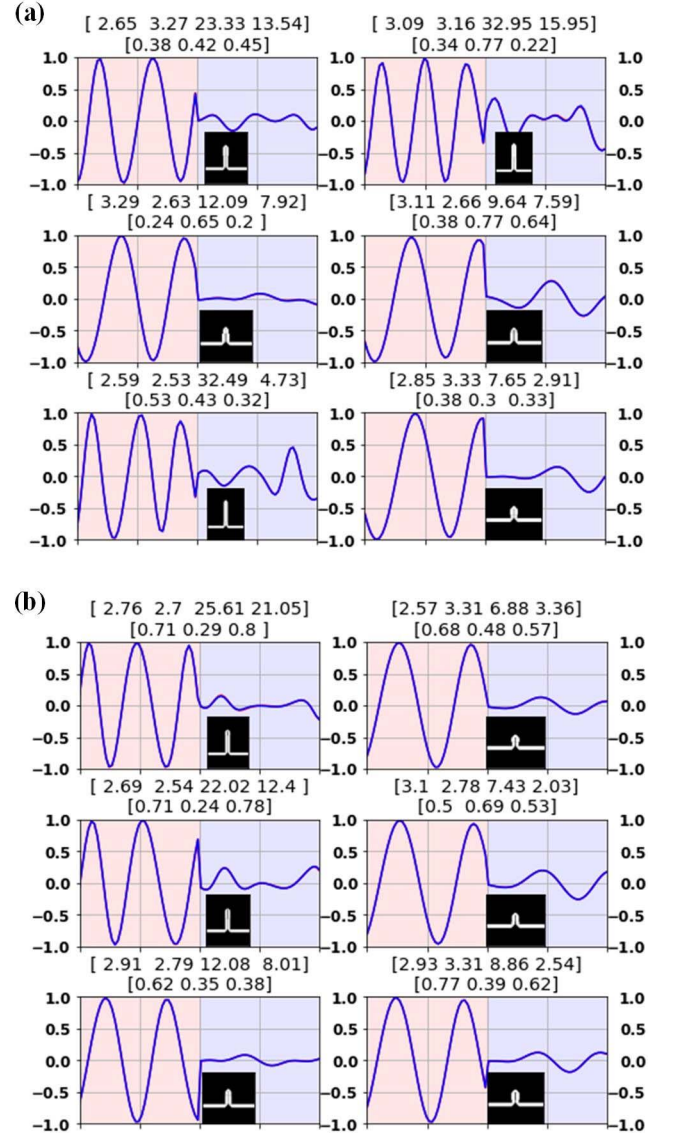


Fig. 10. Additional prediction examples generated with the dual-section PNNs. (a) Real part prediction examples. (b) Imaginary part prediction examples.

#### C. Additional Samples of the PNN for Dual-Section Schiffman Phase Shifters

In each panel of Fig. 10, the red curve represents the PNN predicted values. The blue curves depict numerically simulated values obtained with the commercial frequency domain solver

TABLE III  
DETAILED DIMENSIONS OF THE PHASE-SHIFTER DESIGNS IN FIG. 7

Unit: mm	Phase shifter #1							Additional 50Ω line
	W1	W2	L1	L2	L3	D1	D2	
180° (60% BW)	3.21	2.8	16.91	4.35	0.68	0.78	0.2	9.08
Phase shifter #2								
	W1	W2	L1	L2	L3	D1	D2	
	2.74	3.29	24.82	17.25	0.22	0.2	0.8	

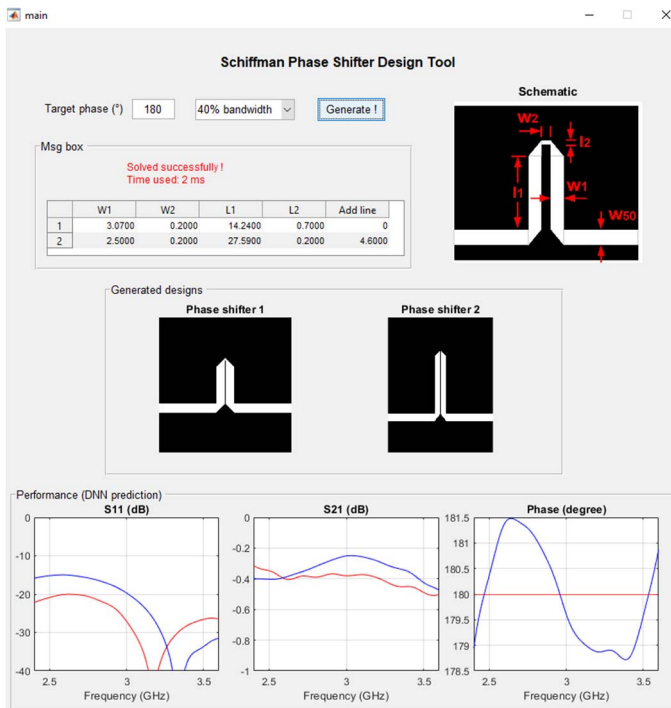


Fig. 11. User interface for the Schiffman phase shifter inverse design network. Target phase ( $0^\circ$ – $180^\circ$ ) and fractional bandwidth (40% or 60%) are needed to generate the inverse phase shifter design. The design parameters and layout of the generated designs, along with the predicted performances, are calculated simultaneously. A  $180^\circ$  phase shifter with 40% fractional bandwidth was designed using this system as an example.

(CST Microwave Studio). Reflection coefficients are highlighted in orange and transmission coefficients are highlighted in cyan. Randomly generated design parameters, including  $W_1$ ,  $W_2$ ,  $L_1$ ,  $L_2$ ,  $L_3$ ,  $D_1$ , and  $D_2$  (in mm), are shown at the top of each panel (in the above order).

#### D. Network Deployment

To better showcase the time efficiency and accuracy of the proposed method, we have developed the fully trained DNN model and built a Schiffman phase-shifter inverse design system (see Fig. 11) using MATLAB built-in app designer. This inverse design system takes the target phase shift and desired fractional bandwidth as input, and generates the design schematic, design parameters, as well as the predicted performances of generated designs as output. The workflow of this design system is as follows: 1) the target phase and fractional bandwidth input by the user is fed to the inverse design network, which generates the design parameters of two

differential phase-shifter structures (shown in the center box of Fig. 11); and 2) performance of these two structures including the  $S_{11}$ ,  $S_{21}$  and differential phase are calculated using the pretrained PNNs and shown in the performance box on the bottom. The overall design time is displayed in the message box, which is normally milliseconds.

#### ACKNOWLEDGMENT

The datasets used during training and the deployed Schiffman phase-shifter design tool is open source and available at: <https://github.com/SensongAn/DNN-Schiffman-phase-shifter>.

#### REFERENCES

- [1] B. M. Schiffman, "A new class of broad-band microwave  $90^\circ$  phase shifters," *IRE Trans. Microw. Theory Techn.*, vol. 6, no. 2, pp. 232–237, Apr. 1958.
- [2] Q. Liu, Y. Liu, J. Shen, S. Li, C. Yu, and Y. Lu, "Wideband single-layer  $90^\circ$  phase shifter using stepped impedance open stub and coupled-line with weak coupling," *IEEE Microw. Wireless Compon. Lett.*, vol. 24, no. 3, pp. 176–178, Jan. 2014.
- [3] Y. J. Cheng, K. Wu, and W. Hong, "Substrate integrated waveguide (SIW) broadband compensating phase shifter," in *IEEE MTT-S Int. Microw. Symp. Dig.*, Jun. 2009, pp. 845–848.
- [4] B. Schiek and J. Kohler, "A method for broad-band matching of microstrip differential phase shifters," *IEEE Trans. Microw. Theory Techn.*, vol. MTT-25, no. 8, pp. 666–671, Aug. 1977.
- [5] J. L. R. Quirarte and J. P. Starski, "Novel Schiffman phase shifters," *IEEE Trans. Microw. Theory Techn.*, vol. 41, no. 1, pp. 9–14, Jan. 1993.
- [6] C. E. Free and C. S. Aitchison, "Improved analysis and design of coupled-line phase shifters," *IEEE Trans. Microw. Theory Techn.*, vol. 43, no. 9, pp. 2126–2131, Sep. 1995.
- [7] Y.-X. Guo, Z.-Y. Zhang, and L. Ong, "Improved wide-band Schiffman phase shifter," *IEEE Trans. Microw. Theory Techn.*, vol. 54, no. 3, pp. 1196–1200, Mar. 2006.
- [8] Z. Zhang, Y.-C. Jiao, S.-F. Cao, X.-M. Wang, and F.-S. Zhang, "Modified broadband Schiffman phase shifter using dentate microstrip and patterned ground plane," *Prog. Electromagn. Res. Lett.*, vol. 24, pp. 9–16, 2011.
- [9] W. Zhang, Y. Liu, Y. Wu, W. Wang, M. Su, and J. Gao, "A modified coupled-line Schiffman phase shifter with short reference line," *Prog. Electromagn. Res. C*, vol. 54, pp. 17–27, 2014.
- [10] S. EL Marini, J. Zbitou, R. Mandry, A. Errkik, A. Tajmouati, and M. Latrach, "Design of  $45^\circ$  microstrip phase shifter for beam forming network application using parallel coupled lines," in *Proc. Int. Conf. Wireless Technol., Embedded Intell. Syst. (WITS)*, Apr. 2017, pp. 1–3.
- [11] Y.-P. Lyu, L. Zhu, and C.-H. Cheng, "Design and analysis of Schiffman phase shifter under operation of its second phase period," *IEEE Trans. Microw. Theory Techn.*, vol. 66, no. 7, pp. 3263–3269, Jul. 2018.
- [12] L.-L. Qiu, L. Zhu, and Y.-P. Lyu, "Schiffman phase shifters with wide phase shift range under operation of first and second phase periods in a coupled line," *IEEE Trans. Microw. Theory Techn.*, vol. 68, no. 4, pp. 1423–1430, Apr. 2020.
- [13] S. Y. Zheng, S. H. Yeung, W. S. Chan, K. F. Man, and S. H. Leung, "Improved broadband dumb-bell-shaped phase shifter using multi-section stubs," *IET Electron. Lett.*, vol. 44, no. 7, pp. 478–480, Mar. 2008.

- [14] X. Tang and K. Moushaan, "Design of a UWB phase shifter using shunt  $\lambda/4$  stubs," in *IEEE MTT-S Int. Microw. Symp. Dig.*, Jun. 2009, pp. 1021–1024.
- [15] S. Y. Zheng, W. S. Chan, and K. F. Man, "Broadband phase shifter using loaded transmission line," *IEEE Microw. Wireless Compon. Lett.*, vol. 20, no. 9, pp. 498–500, Sep. 2010.
- [16] S. H. Yeung, Z. Mei, T. K. Sarkar, and M. Salazar-Palma, "Design and testing of a single-layer microstrip ultrawideband 90° differential phase shifter," *IEEE Microw. Wireless Compon. Lett.*, vol. 23, no. 3, pp. 122–124, Mar. 2013.
- [17] S. An, M. Badar, and Q. Zhu, "Generalized analysis method for a class of novel wideband loaded-stub phase shifters," *Radioengineering*, vol. 24, no. 4, p. 927, 2015.
- [18] B. Muneer, A. Sensong, A. W. Umrani, F. K. Shaikh, and U. Ahmed, "A generalized approach to analyze broadband arrow-shaped loaded-stub phase shifters," in *Proc. Adv. Electromagn. Symp. (AES)*, Málaga, Spain, Jul. 2016.
- [19] A. M. Abbosh, "Ultra-wideband phase shifters," *IEEE Trans. Microw. Theory Techn.*, vol. 55, no. 9, pp. 1935–1941, Sep. 2007.
- [20] A. M. Abbosh, "Broadband fixed phase shifters," *IEEE Microw. Wireless Compon. Lett.*, vol. 21, no. 1, pp. 22–24, Jan. 2010.
- [21] Y. Wang, M. Bialkowski, and A. Abbosh, "Double microstrip-slot transitions for broadband  $\pm 90^\circ$  microstrip phase shifters," *IEEE Microw. Wireless Compon. Lett.*, vol. 22, no. 2, pp. 58–60, Jan. 2012.
- [22] Y. S. Wong, S. Y. Zheng, and W. S. Chan, "Multi-way and poly-phase aligned feed-forward differential phase shifters," *IEEE Trans. Microw. Theory Techn.*, vol. 62, no. 6, pp. 1312–1321, Jun. 2014.
- [23] Y.-P. Lyu, L. Zhu, Q.-S. Wu, and C.-H. Cheng, "Proposal and synthesis design of wideband phase shifters on multimode resonator," *IEEE Trans. Microw. Theory Techn.*, vol. 64, no. 12, pp. 4211–4221, Dec. 2016.
- [24] J. Zhou, H. J. Qian, and X. Luo, "Compact wideband phase shifter using microstrip self-coupled line and broadside-coupled microstrip/CPW for multiphase feed-network," *IEEE Microw. Wireless Compon. Lett.*, vol. 27, no. 9, pp. 791–793, Sep. 2017.
- [25] P. M. Watson, K. C. Gupta, and R. L. Mahajan, "Applications of knowledge-based artificial neural network modeling to microwave components," *Int. J. RF Microw. Comput. Aided Eng.*, vol. 9, no. 3, pp. 254–260, May 1999.
- [26] P. M. Watson, K. C. Gupta, and R. L. Mahajan, "Development of knowledge based artificial neural network models for microwave components," in *IEEE MTT-S Int. Microw. Symp. Dig.*, vol. 1, Jun. 1998, pp. 9–12.
- [27] V. K. Devabhaktuni, M. C. E. Yagoub, Y. Fang, J. Xu, and Q.-J. Zhang, "Neural networks for microwave modeling: Model development issues and nonlinear modeling techniques," *Int. J. RF Microw. Comput.-Aided Eng.*, vol. 11, no. 1, pp. 4–21, Jan. 2001.
- [28] H. J. Delgado, M. H. Thrusby, and F. M. Ham, "A novel neural network for the synthesis of antennas and microwave devices," *IEEE Trans. Neural Netw.*, vol. 16, no. 6, pp. 1590–1600, Nov. 2005.
- [29] Z. Zhang, Q. S. Cheng, H. Chen, and F. Jiang, "An efficient hybrid sampling method for neural network-based microwave component modeling and optimization," *IEEE Microw. Wireless Compon. Lett.*, vol. 30, no. 7, pp. 625–628, Jul. 2020.
- [30] Q. J. Zhang, K. C. Gupta, and V. K. Devabhaktuni, "Artificial neural networks for RF and microwave design—from theory to practice," *IEEE Trans. Microw. Theory Techn.*, vol. 51, no. 4, pp. 1339–1350, Apr. 2003.
- [31] Y. Cao, G. Wang, and Q.-J. Zhang, "A new training approach for parametric modeling of microwave passive components using combined neural networks and transfer functions," *IEEE Trans. Microw. Theory Techn.*, vol. 57, no. 11, pp. 2727–2742, Nov. 2009.
- [32] W. Na, W. Zhang, S. Yan, F. Feng, W. Zhang, and Y. Zhang, "Automated neural network-based multiphysics parametric modeling of microwave components," *IEEE Access*, vol. 7, pp. 141153–141160, 2019.
- [33] C. Zhang, J. Jin, W. Na, Q. J. Zhang, and M. Yu, "Multivalued neural network inverse modeling and applications to microwave filters," *IEEE Trans. Microw. Theory Techn.*, vol. 66, no. 8, pp. 3781–3797, Aug. 2018.
- [34] J. Jin *et al.*, "Recent advances in neural network-based inverse modeling techniques for microwave applications," *Int. J. Numer. Modelling. Electron. Netw. Devices Fields*, vol. 33, no. 6, p. e2732, Nov. 2020.
- [35] F. Feng, J. Zhang, W. Zhang, Z. Zhao, J. Jin, and Q. Zhang, "Recent advances in parametric modeling of microwave components using combined neural network and transfer function," *Int. J. Numer. Modelling. Electron. Netw. Devices Fields*, vol. 33, no. 6, p. e2733, Nov. 2020.
- [36] S. So, J. Mun, and J. Rho, "Simultaneous inverse design of materials and structures via deep learning: Demonstration of dipole resonance engineering using core-shell nanoparticles," *ACS Appl. Mater. Interfaces*, vol. 11, no. 27, pp. 24264–24268, 2019.
- [37] D. Liu, Y. Tan, E. Khoram, and Z. Yu, "Training deep neural networks for the inverse design of nanophotonic structures," *ACS Photon.*, vol. 5, no. 4, pp. 1365–1369, Apr. 2018.
- [38] S. An *et al.*, "A deep learning approach for objective-driven all-dielectric metasurface design," *ACS Photon.*, vol. 6, no. 12, pp. 3196–3207, 2019.
- [39] S. An *et al.*, "Deep learning modeling approach for metasurfaces with high degrees of freedom," *Opt. Exp.*, vol. 28, no. 21, p. 31932, Oct. 2020, doi: [10.1364/oe.401960](https://doi.org/10.1364/oe.401960).
- [40] S. An *et al.*, "Multifunctional metasurface design with a generative adversarial network," *Adv. Opt. Mater.*, vol. 9, no. 5, Mar. 2021, Art. no. 2001433.
- [41] H. M. El Mislimani, T. Naous, and S. K. Al Khatib, "A review on the design and optimization of antennas using machine learning algorithms and techniques," *Int. J. RF Microw. Comput.-Aided Eng.*, vol. 30, no. 10, Oct. 2020.
- [42] A. Massa, D. Marcantonio, X. Chen, M. Li, and M. Salucci, "DNNs as applied to electromagnetics, antennas, and propagation—A review," *IEEE Antennas Wireless Propag. Lett.*, vol. 18, no. 11, pp. 2225–2229, Nov. 2019.
- [43] J. Jin, C. Zhang, F. Feng, W. Na, J. Ma, and Q.-J. Zhang, "Deep neural network technique for high-dimensional microwave modeling and applications to parameter extraction of microwave filters," *IEEE Trans. Microw. Theory Techn.*, vol. 67, no. 10, pp. 4140–4155, Oct. 2019.
- [44] J. Jin, F. Feng, J. Zhang, S. Yan, W. Na, and Q. Zhang, "A novel deep neural network topology for parametric modeling of passive microwave components," *IEEE Access*, vol. 8, pp. 82273–82285, 2020.
- [45] G. Cybenko, "Approximation by superpositions of a sigmoidal function," *Math. Control. Signals Syst.*, vol. 2, no. 4, pp. 303–314, 1989.
- [46] K. Hornik, M. Stinchcombe, and H. White, "Multilayer feedforward networks are universal approximators," *Neural Netw.*, vol. 2, no. 5, pp. 359–366, Jan. 1989.
- [47] M. Sorn, R. Lech, and J. Mazur, "Simulation and experiment of a compact wideband 90° differential phase shifter," *IEEE Trans. Microw. Theory Techn.*, vol. 60, no. 3, pp. 494–501, Nov. 2011.
- [48] X. Tang and K. Moushaan, "Phase-shifter design using phase-slope alignment with grounded shunt  $\lambda/4$  stubs," *IEEE Trans. Microw. Theory Techn.*, vol. 58, no. 6, pp. 1573–1583, May 2010.



**Sensong An** received the B.Eng. and M.Eng. degrees from the University of Science and Technology of China, Hefei, China, in 2013 and 2016, respectively, and the Ph.D. degree from the University of Massachusetts at Lowell, Lowell, MA, USA, in 2021.

He is currently a Post-Doctoral Researcher with the Department of Material Science and Engineering, Massachusetts Institute of Technology, Cambridge, MA. His research interests are in the area of applied electromagnetics, including metasurfaces and metamaterials (invisible, infrared, and RF), passive microwave circuits and components, phase change materials, and inverse design approaches enabled by deep learning techniques.



**Bowen Zheng** received the B.S. degree in electrical engineering from Southeast University, Nanjing, China, in 2014, the M.S. degree in electrical and computer engineering from the University of Maryland, College Park, MD, USA, in 2016, and the Ph.D. degree in electrical engineering from the University of Massachusetts at Lowell, Lowell, MA, USA, in 2021.

He is currently working as a Research Scientist with the Department of Electrical and Computer Engineering, University of Massachusetts at Lowell. His current research interests include the design and measurement of tunable electromagnetic devices.



**Hong Tang** received the B.Sc. degree in optoelectronic information science and engineering from Huazhong University of Science and Technology, Wuhan, China, in 2017.

He has been serving as a Research Assistant with the University of Massachusetts at Lowell, Lowell, MA, USA, since 2017. His current research interests include wideband antenna array, millimeter-wave systems, and flexible systems.



**Yunxi Dong** received the B.S. degree in finance from the University of Oregon, Eugene, OR, USA, in 2016, and the M.S. degree in data science from Syracuse University, Syracuse, NY, USA, in 2020. He is currently pursuing the Ph.D. degree in computer engineering with the University of Massachusetts at Lowell, MA, USA.

His research interests include the artificial intelligence for metasurface, metalens design, tunable metasurface, and deep learning for image reconstruction.



**Hang Li** received the B.S. degree in physics from Jilin University, Changchun, China, in 2016. She is currently pursuing the Ph.D. degree in the field of metasurfaces devices with the Department of Electrical and Computer Engineering, University of Massachusetts at Lowell, Lowell, MA, USA.

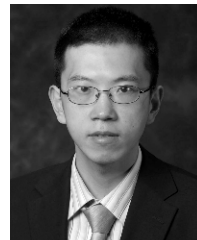
In 2017, she joined the Department of Electrical and Computer Engineering, University of Massachusetts Lowell. Her current research interests include photonic device, laser devices, and multifunctional optical devices based on metasurfaces.

She is an expertise in nanotechnologies and nanofabrication.



**Mohammad Haerinia** (Student Member, IEEE) received the B.Sc. and M.Sc. degrees in electrical engineering from Shahid Beheshti University, Tehran, Iran, in 2014 and 2016, respectively, and the second M.Sc. degree in biomedical engineering from the University of North Dakota, Grand Forks, ND, USA, in 2019. He is currently pursuing the Ph.D. degree in electrical engineering with the University of Massachusetts at Lowell, Lowell, MA, USA.

His research interests include the multidisciplinary areas of applied electromagnetics, including medical optics, metasurfaces, wireless power transfer (WPT), and WPT for medical applications.

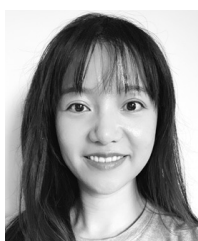


**Hualiang Zhang** (Senior Member, IEEE) received the B.S. degree in electrical engineering from the University of Science and Technology of China, Hefei, China, in 2003, and the Ph.D. degree in electrical and computer engineering from The Hong Kong University of Science and Technology, Hong Kong, in 2007.

From 2007 to 2009, he was a Post-Doctoral Research Associate with The University of Arizona, Tucson, AZ, USA. From 2009 to 2016, he was an Assistant Professor and then an Associate Professor

with the University of North Texas, Denton, TX, USA. He is currently a Professor with the Department of Electrical and Computer Engineering, University of Massachusetts at Lowell, Lowell, MA, USA. He has coauthored over 250 journal articles and conference papers. His research interests include RF/microwave/millimeter-wave circuits and systems, antennas, metasurfaces and metamaterials, nano-photonics and optoelectronics in both rigid and flexible substrates, as well as their applications, covering the frequency range from RF/microwave and THz to infrared and visible.

Dr. Zhang serves as the Subcommittee Chair of the IEEE International Microwave Symposium and a Technical Committee Member of several major technical conferences, as well as an Associate Editor for *International Journal of Numerical Modelling: Electronic Networks, Devices and Fields*.



**Li Zhou** received the B.Eng. degree from Nanjing Agricultural University, Nanjing, China, in 2012, and the M.Sc. degree from the University of Leicester, Leicester, U.K., in 2015. She is currently pursuing the Ph.D. degree in computer engineering with the University of Massachusetts at Lowell, Lowell, MA, USA.

Her research interests include the designing and developing of machine learning models and deep learning models with multimodality datasets.